ACS OMEGA

http://pubs.acs.org/journal/acsodf

Article

Solution-Processed Organic Photodetectors with Renewable Materials

Yu-Chi Chang,* Ting-Yun Wang, and Hong-Bing Chen

Cite This: *ACS Omega* 2022, 7, 10622−10626

Read Online

ACCESS | Metrics & More | Article Recommendations

ABSTRACT: An organic photodetector prepared by a simple solution method based on renewable citrus pectin with an optimized concentration of aluminum nitrate (AlC05) is introduced herein. The effects of different concentrations of aluminum nitrate on the morphology and optical properties were investigated through various characterization methods. An AlC concentration of 0.5 mg/mL was found to provide the highest on/off ratio and acceptable rise and decay times. Also, the optimized device (Al/AlC0.5/ITO) exhibited good stability and repeatability at a 0.1 V bias under 440 nm visible light. Based on these results, citrus pectin materials were successfully used to fabricate an organic photodetector with a simple and cost-efficient fabrication process, while taking into account environmental commitments.

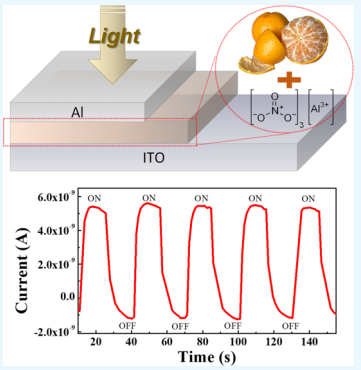

1. INTRODUCTION

To reduce electronic wastes, the implementation of electronic devices consisting of materials that can be broken down into bio-derived blocks has become an important requirement. Citrus pectin is a nontoxic biodegradable material and an ideal candidate for the fabrication of eco-friendly electronic devices.[1] In general, inorganic materials such as Si, Ge, and GalnAs are widely applied in photodetectors. Although inorganic materials exhibit good device performance, citrus materials have a low cost, simple fabrication, and excellent mechanical characteristics; moreover, they are renewable and can be used in low-temperature solutions.[2−4] Few studies have been conducted on the use of renewable materials as sensing layers for the discussion of their photoelectric characteristics.[5,6] In our previous work,[7] an on/off ratio of over 10^4 was achieved for the Al/citrus/ITO structure. However, the application of citrus pectin-based electro-optical devices has not yet been widely discussed. In addition, the Al/citrus/ITO structure does not exhibit light-sensitive properties. Organic materials are the current research trend in light-receiving materials.[8] Organic photodetectors (OPDs) have many advantages, such as a low-temperature solution process, low cost, and an adjustable absorption response band.[9,10] They are widely in demand for visible detector applications, such as light detection and range, time-of-flight sensors, and structured light sensors for cameras.[11−16] During the fabrication of OPDs, their photoelectric conversion efficiency can be effectively improved based on different structural combinations and selection of light-receiving materials in the bulk heterojunction layer. This layer is located between the hole- and electron-blocking layers.[17,18] This structure has a larger contact interface between the donor and the acceptor, making the separation of excitons from the interface for charge separation easy. To maintain the balance of the electron−hole mobility, the donor and acceptor materials must be mixed in an appropriate ratio. This setup can effectively separate the electrons and holes at the interface and prevent recombination.[19−23] Studies have reported that if the electron donor and electron acceptor ratio is effectively maintained, a highly efficient light-sensitive element can be obtained. Therefore, a biodegradable material of AlC prepared by a low-temperature solution in the Al/AlC/ITO structure is used herein to achieve an OPD with high photoelectric conversion efficiency. To investigate the mechanism of the citrus-based photodetector, the relationship between the concentration of the Al salt and the device performance is also discussed in this paper.

2. EXPERIMENTAL DETAILS

Device Fabrication. Figure 1a shows the fabrication process of OPD. The OPD consisted of a metal/insulator/metal structure with AlC as the dielectric layer. First, the AlC solutions were prepared by mixing different amounts of aluminum nitrate salt powder, DI water, and citrus powder.

Received: January 10, 2022
Accepted: February 28, 2022
Published: March 17, 2022

https://doi.org/10.1021/acsomega.2c00178
ACS Omega 2022, 7, 10622−10626

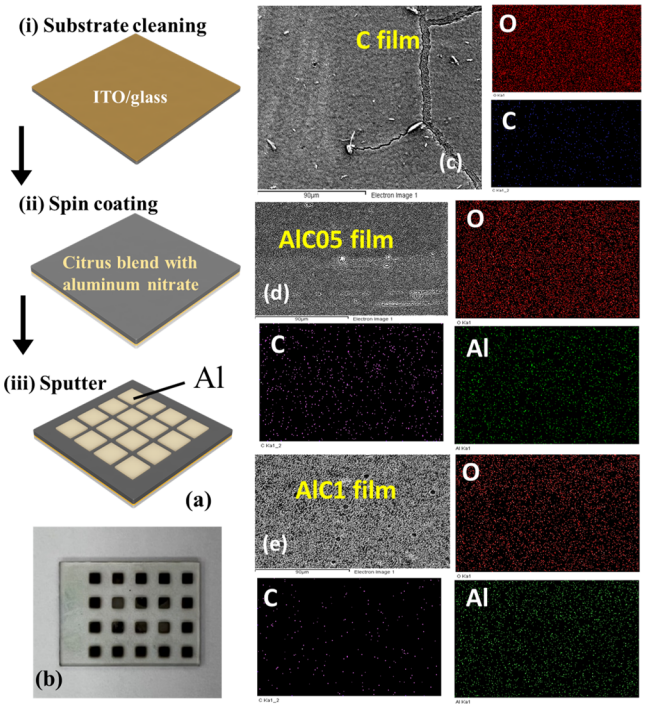

Figure 1. (a) Fabrication processes of the OPD. (b) Optical image of the organic photodetector. SEM topographic and EDS elemental mapping images of (c) AlC0, (d) AlC05, and (e) AlC1 thin films.

The concentrations of the AlC solutions were adjusted to 0, 0.5, and 1.0 mg/mL, hereafter denoted as AlC0, AlC05, and AlC1, respectively. Subsequently, the solution was spin-coated onto the ITO/glass surface, followed by baking at 60 °C for 30 min in air. Finally, a shadow mask was placed onto the dielectric layers, then placed in a radio frequency (RF) magnetron sputtering system using the Ar gas with a working pressure of 20 mTorr and an RF power of 250 W. After sputtering, the shadow mask was removed to obtain an Al square-shaped pattern layer, as shown in Figure 1b. The top Al electrode area was 3 mm^2. The device was not packaged because Al has a slight oxidation resistance and can protect the photodetector (slight loss).[24] Figure 1c–e presents the scanning electron microscopy (SEM) topographic and the energy dispersive X-ray spectroscopy (EDS) element mapping images of the AlC0, AlC05, and AlC1 thin films, respectively. In addition, as shown in Figure 1d, the uniform distribution of Al in the AlC05 thin film can be observed.

Instrumentation. The surface morphology and the roughness of the samples were determined by atomic force microscopy (AFM, Dimension ICON with Nano Scope V controller, Bruker, Karlsruhe, Germany) in air. The current–voltage (I–V) characteristics and the time response of the proposed OPD were measured using a source-measuring unit in the dark and under blue light excitation (λ = 400–490 nm) through the top electrode side. Transmission electron microscopy analysis was conducted using a 200 kV JEM-2100F electron microscope (Jeol, Tokyo, Japan). X-ray photoelectron spectroscopy (XPS) was performed using a PHI 5000 VersaProbe (Kanagawa, Japan).

3. RESULTS AND DISCUSSION

XPS analysis was carried out to investigate the elemental composition of the films and examine their chemical states by making the inner electronic state reflect the state of the outer electrons. Four elements were observed, namely, C, N, O, and Al, where the C element observed from the full scan was adventitious carbon. Therefore, this work demonstrated that the citrus layer is mainly organic. Different concentrations of aluminum nitrate of 0 M [only 1% of citrus (AlC0)], 0.5 M (AlC05), and 1.0 M (AlC1) were used. From the obtained XPS survey scanning, the Al/citrus: Al $(NO_3)_3$/ITO ratio was derived and the composition of the device was verified. In the device with a concentration of 1% citrus, the elemental ratios of C, O, N, and Al were 57.5, 33.7, 8.7, and 0.1%, respectively. In the two other devices with AlC05 and AlC1, the elemental ratios were 49.3, 36.0, 8.9, and 5.9% and 42.5, 39.0, 12.5, and 5.8%. The strong peaks centered at 75 eV for the surface indicate the presence of Al. Figure 2a shows that the

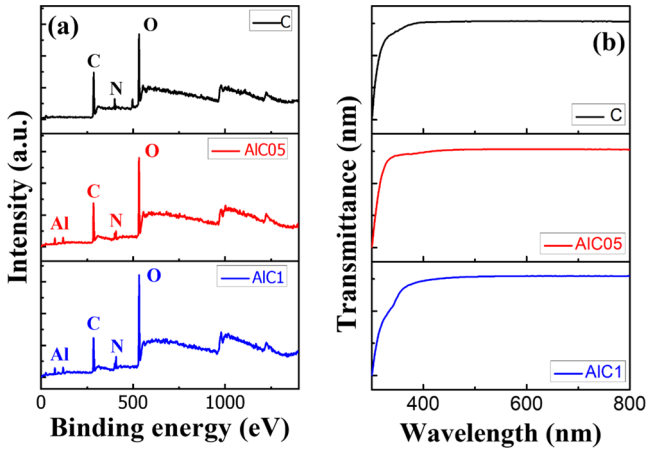

Figure 2. (a) XPS and (b) UV–vis transmittance spectra of AlC0, AlC05, and AlC1 thin films.

proportions of C, N, and O in the three elements are similar. The most significant difference is that the Al content clearly increased by 6% in the citrus mixed with different concentrations of aluminum nitrate. Figure 2b presents the UV–vis transmission spectra of the Al-embedded citrus thin film produced by the solution method and with different concentrations of aluminum nitrate. The ultraviolet–visible transmission spectra were measured at room temperature (approximately 24.5–26 °C) using a spectrophotometer and a quartz cuvette with an optical path of 10 mm. Compared with the different concentrations of aluminum nitrate in the device, the normalized values of the transmission spectra of AlC0, AlC05, and AlC1 were 0.81, 0.83, and 0.83, respectively. The results show that AlC on the insulating layer with different concentrations has the same transmission spectrum in the wavelength range of 400–800 nm. Figure 3a–c shows the respective topographic images of the AlC0, AlC05, and AlC1 layers captured using an atomic force microscope operating in the tapping mode. The roughness values of the AlC0, AlC05, and AlC1 thin films were 8.01, 34.3, and 10.04 nm, respectively. Figure 3d shows the Fourier-transform infrared spectra of the AlC05 thin films. The absorption bands at 1635 cm^{-1} are related to the −C(=O)−O stretching of the carboxylate groups and the C=O stretching vibrations of the carboxylic acid.[25] The peaks at 1319 cm^{-1} are related to the −O−C stretching of the aryl–alkyl ether linkage.[26] The bands at approximately 1000–1100 cm^{-1} could be attributed to the C−O−H alcohol bonds of the saturated carbon as well as the

https://doi.org/10.1021/acsomega.2c00178
ACS Omega 2022, 7, 10622–10626

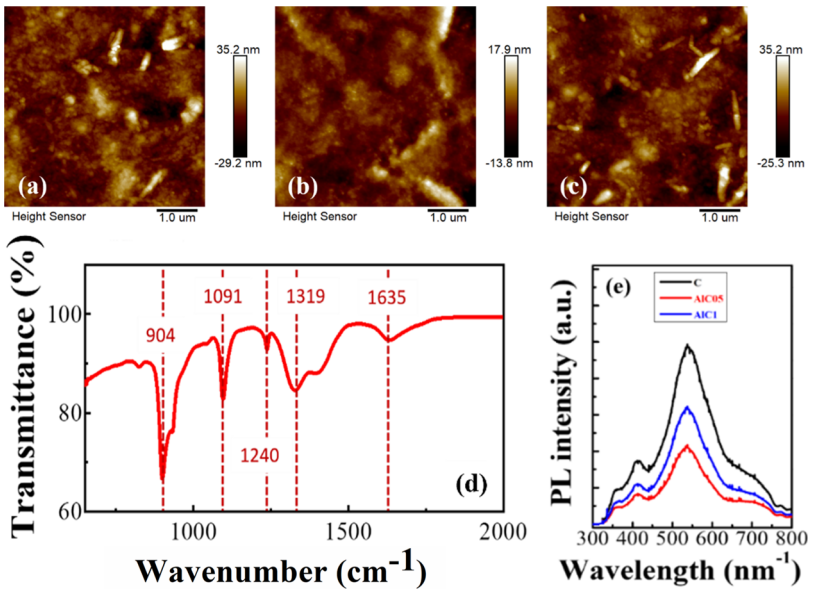

Figure 3. AFM images of AlC at different concentrations of (a) 0, (b) 5, and (c) 1 M, respectively. (d) FTIR spectrum of the AlC05 thin film and (e) comparison of the PL spectra of the thin films of citrus pectin with different concentrations of aluminum nitrate.

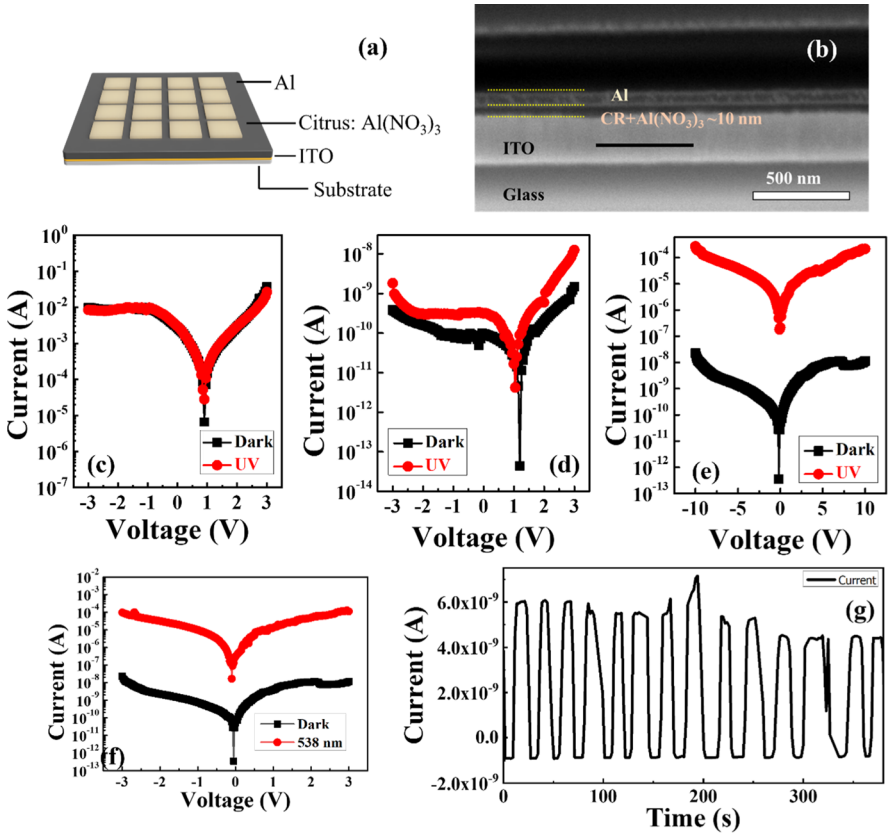

Figure 4. (a) Device schematics of the organic photodetector with aluminum nitrate and (b) FIB cross-section micrographs. Photocurrent and dark-current curves of (c) AlC0, (d) AlC1, and (e) AlC05. (f) Photocurrent and dark-current curves and (g) time-dependent photoresponse while AlC05 was irradiated with a pumping light of 538 nm wavelength.

C−O stretching and deformation. Figure 3e shows the photoluminescence (PL) spectra of the AlC0, AlC05, and AlC1 thin films. The PL spectral data were obtained at an excitation wavelength of 325 nm. The emission peak of citrus/Al $(NO_3)_3$ was centered at 538 nm, which corresponds to the green light emission. The quenching phenomenon and the reduction in the full width at half-maximum (FWHM) can be observed. The FWHM values for the AlC0, AlC05, and AlC1 thin films were 93, 81, and 72 keV, respectively. The data above show that the smaller the FWHM value corresponds to a narrower waveform and a better energy resolution. Figure 4a presents the structure of the AlC05 device. In Figure 4b, the

https://doi.org/10.1021/acsomega.2c00178
ACS Omega 2022, 7, 10622−10626

FIB diagram shows that the AlC05 film prepared by the solution method was of approximately 10 nm. In this paper, an OPD manufacturing process was developed to create a very thin AlC05 film using an organic polymer, and the $I-V$ curve was measured to characterize the organic polymer photosensitive layer. In addition, the measurement results were determined by two index values, photocurrent and dark current (I_{light}/I_{dark}), to observe the trend of light and dark currents at different voltages. The OPD without the mixture (the active layer only with citrus) was selected as a reference device (AlC0), and the OPDs with doping concentrations of 0.5 M (AlC05) and 1 M (AlC1) were used as comparison devices. Figure4c–e shows the $I-V$ curves of AlC0, AlC05, and AlC1 obtained in the dark and under excitation with a pumping beam of 365 nm wavelength. On the one hand, the values of I_{Light} of AlC0, AlC05, and AlC1 were around 10^{-2}, 2.5×10^{-10}, and 10^{-5} A, respectively. On the other hand, the values of I_{Dark} of AlC0, AlC05, and AlC1 were around 10^{-2}, 6×10^{-10}, and 10^{-9} A, respectively. Figure4f,g shows the $I-V$ curves recorded in the dark and under excitation with a pumping beam of 538 nm wavelength and the long-term cycling performance ($I-T$), respectively. I_{Light} and I_{Dark} were around 3.4×10^{-4} and 2.4×10^{-7} A, respectively. In addition, Figure 5a shows that the

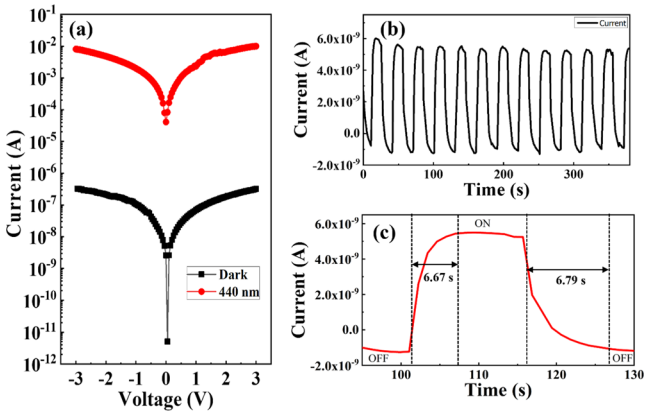

Figure 5. (a) $I-V$ performance and (b) time-dependent photoresponse of AlC05. (c) Enlarged view of the time-response spectrum.

values of I_{Light} and I_{Dark} of AlC05 obtained under excitation with a pumping beam of 440 nm wavelength and in the dark, which were 10^{-2} and 3.2×10^{-6} A, respectively. Compared with the reported OPDs 5 and 6, the AlC05 photodetector had a relatively high on/off ratio. Based on the $I-V$ results, the dynamic value of wavelength 538 nm was lower than the value of wavelength 440 nm. In addition, the $I-T$ curves obtained under excitation with a pumping beam of 538 nm wavelength exhibited an unstable dynamic photoresponse. Therefore, the wavelength of 440 nm was selected as the measurement condition in this paper. AlC05 had better properties because the uniform distribution of Al particles enabled the transfer of electrons and holes easier. However, when the Al concentration was increased, conductivity also increased, following which the dark current increased, resulting in a decrease in the on/off ratio. This phenomenon limited the photoelectric conversion efficiency of the device (photo-to-volt effect) and made the I_{Light} value and I_{Dark} characteristics of the device insignificant. In addition, in our proposed device, the citrus pectin (acceptor) and a sufficient concentration of aluminum nitrate (donor) were uniformly mixed. Thus, the photosensitive layer became a single-layered heterojunction (bulk layer heterojunction), and the donor was uniformly formed in the acceptor. The mesh path allowed the carrier to transfer easily to the corresponding electrodes and smoothly produce a photovoltaic special effect, clarifying the characteristics of light and dark currents. In modern technology applications, the repeatability and the stability of photoelectric sensors play a crucial role in determining their function and response speed. The time response of the UV of OPD was measured at 0.1 V bias under 440 nm visible light with an on/off interval of 15 s. From the enlarged rising and decaying edges of the photocurrent response in Figure 5c, the time taken for the current to increase from 10 to 90% of the peak value, or vice versa, was defined as the rise or decay time. The rise and decay times of the AlC05 OPD were approximately 6.67 and 6.79 s, respectively, indicating the existence of two channels for the recombination of holes. The issues of OPD were structural imperfection, thermal damage, and diffusion phenomena, which would result in physical or chemical wear and a slow response.[27] Figure 5b shows a long-term cycling performance ($I-T$), which was measured under excitation with a pumping beam of 440 nm wavelength for 380 s. A stable dynamic photoresponse can be observed. These results provide one more possibility for the application of renewable materials in optic electronics.

4. CONCLUSIONS

In summary, according to the experimental results, when the active layer concentration was 1% citrus blended with aluminum nitrate (0.5 M) and the layer thickness was ∼10 nm, a high I_{Light}/I_{Dark} performance was achieved with the renewable material. This bulk layer heterojunction of the OPD was fabricated using rapid spin-coating and thermal evaporation. By applying this renewable material consisting of citrus pectin and aluminum nitrate as the active layer of the OPD, an appropriate amount of electron acceptor and donor can transfer to the network channel. This setup can efficiently transfer the separated charges to the corresponding electrodes. Moreover, AlC05 had an I_{Light} of 10^{-5} and an I_{Dark} of 10^{-9}, indicating a higher sensing ability than the reference device and a successful photovoltaic effect. The AlC thin film produced by the solution method, where the metal salts were dissolved in citrus pectin, was presented. OPD was characterized under visible light irradiation after blending aluminum nitrate with the citrus pectin layer. Overall, the emerging organic visible OPD based on the natural citrus pectin material may help in developing low-cost, environmentally friendly devices. Photodetector optimization via biomaterial engineering enables a deeper understanding of the material parameters controlling the device performances, enabling their better exploration for future bioelectronics.

AUTHOR INFORMATION

Corresponding Author

Yu-Chi Chang − *Department of Engineering Science, National Cheng Kung University, Tainan 70101, Taiwan;*
orcid.org/0000-0003-2253-935X;
Email: christina780712@gmail.com

Authors

Ting-Yun Wang − *Department of Engineering Science, National Cheng Kung University, Tainan 70101, Taiwan*

https://doi.org/10.1021/acsomega.2c00178
ACS Omega 2022, 7, 10622−10626

Hong-Bing Chen − *Department of Engineering Science, National Cheng Kung University, Tainan 70101, Taiwan;* orcid.org/0000-0001-7244-0708

Complete contact information is available at: https://pubs.acs.org/10.1021/acsomega.2c00178

Notes

The authors declare no competing financial interest.

■ ACKNOWLEDGMENTS

This research was sponsored by the Ministry of Science and Technology of Taiwan under grant no. MOST 108-2636-E-006-008. We also thank Mr. Jui-Chin Lee (Instrument Center NCKU) for sample preparation and XPS investigation.

■ REFERENCES

(1) Bockarjova, M.; Botzen, W. J. W.; van Schie, M. H.; Koetse, M. J. Property Price Effects of Green Interventions in Cities: A Meta-Analysis and Implications for Gentrification. *Environ. Sci. Policy* **2020**, *112*, 293−304.

(2) Liu, X.; Lin, Y.; Liao, Y.; Wu, J.; Zheng, Y. Recent Advances in Organic Near-Infrared Photodiodes. *J. Mater. Chem. C* **2018**, *6*, 3499−3513.

(3) Wu, Z.; Yao, W.; London, A. E.; Azoulay, J. D.; Ng, T. N. Elucidating the Detectivity Limits in Shortwave Infrared Organic Photodiodes. *Adv. Funct. Mater.* **2018**, *28*, 1800391.

(4) Lin, Q.; Armin, A.; Burn, P. L.; Meredith, P. Near Infrared Photodetectors Based on Sub-Gap Absorption in Organohalide Perovskite Single Crystals. *Laser Photonics Rev.* **2016**, *10*, 1047−1053.

(5) Tang, X.; Zu, Z.; Shao, H.; Hu, W.; Zhou, M.; Deng, M.; Chen, W.; Zang, Z.; Zhu, T.; Xue, J. All-Inorganic Perovskite CsPb(Br/I)3 Nanorods for Optoelectronic Application. *Nanoscale* **2016**, *8*, 15158−15161.

(6) Wang, X.; Huang, J.; Han, S.; Yu, J. High Photoresponse Inverted Ultraviolet Photodectectors Consisting of Iridium Phosphor Doped into Poly(N-Vinylcarbazole) Polymeric Matrix. *Appl. Phys. Lett.* **2014**, *104*, 173304.

(7) Ciriminna, R.; Fidalgo, A.; Delisi, R.; Carnaroglio, D.; Grillo, G.; Cravotto, G.; Tamburino, A.; Ilharco, L. M.; Pagliaro, M. High-Quality Essential Oils Extracted by an Eco-Friendly Process from Different Citrus Fruits and Fruit Regions. *ACS Sustainable Chem. Eng.* **2017**, *5*, 5578−5587.

(8) Ren, H.; Chen, J. D.; Li, Y. Q.; Tang, J. X. Recent Progress in Organic Photodetectors and Their Applications. *Adv. Sci.* **2021**, *8*, 2002418.

(9) Renshaw, C. K.; Xu, X.; Forrest, S. R. A Monolithically Integrated Organic Photodetector and Thin Film Transistor. *Org. Electron.* **2010**, *11*, 175−178.

(10) Lee, S.; Seong, H.; Im, S. G.; Moon, H.; Yoo, S. Organic Flash Memory on Various Flexible Substrates for Foldable and Disposable Electronics. *Nat. Commun.* **2017**, *8*, 725.

(11) Ghoneim, M.; Hussain, M. Review on Physically Flexible Nonvolatile Memory for Internet of Everything Electronics. *Electronics* **2015**, *4*, 424−479.

(12) Alzahrani, H.; Sulaiman, K.; Mahmoud, A. Y.; Bahabry, R. R. Study of Organic Visible-Blind Photodetector Based on Alq3:NPD Blend for Application in near-Ultraviolet Detection. *Opt. Mater. (Amsterdam, Neth.)* **2020**, *110*, 110490.

(13) Spanoudaki, V. C.; Levin, C. S. Photo-Detectors for Time of Flight Positron Emission Tomography (ToF-PET). *Sensors* **2010**, *10*, 10484−10505.

(14) Wang, C.; Zhang, X.; Hu, W. Organic Photodiodes and Phototransistors toward Infrared Detection: Materials, Devices, and Applications. *Chem. Soc. Rev.* **2020**, *49*, 653−670.

(15) Bouquet, G.; Thorstensen, J.; Bakke, K. A. H.; Risholm, P. Design Tool for TOF and SL Based 3D Cameras. *Opt. Express* **2017**, *25*, 27758−27769.

(16) Liu, J.; Wang, Y.; Wen, H.; Bao, Q.; Shen, L.; Ding, L. Organic Photodetectors: Materials, Structures, and Challenges. *Sol. RRL* **2020**, *4*, 2000139.

(17) Royo, S.; Ballesta-Garcia, M. An Overview of Lidar Imaging Systems for Autonomous Vehicles. *Appl. Sci.* **2019**, *9*, 4093.

(18) Udum, Y.; Denk, P.; Adam, G.; Apaydin, D. H.; Nevosad, A.; Teichert, C.; White, M. S.; Sariciftci, N. S.; Scharber, M. C. Inverted Bulk-Heterojunction Solar Cell with Cross-Linked Hole-Blocking Layer. *Org. Electron.* **2014**, *15*, 997−1001.

(19) Peumans, P.; Forrest, S. R. Separation of Geminate Charge-Pairs at Donor-Acceptor Interfaces in Disordered Solids. *Chem. Phys. Lett.* **2004**, *398*, 27−31.

(20) Singh, J.; Narayan, M.; Ompong, D.; Zhu, F. Dissociation of Charge Transfer Excitons at the Donor−Acceptor Interface in Bulk Heterojunction Organic Solar Cells. *J. Mater. Sci.: Mater. Electron.* **2017**, *28*, 7095−7099.

(21) Wang, Q.; Li, Y.; Song, P.; Su, R.; Ma, F.; Yang, Y. Non-Fullerene Acceptor-Based Solar Cells: From Structural Design to Interface Charge Separation and Charge Transport. *Polymers* **2017**, *9*, 692.

(22) Gao, F.; Zhao, Y.; Zhang, X.; You, J. Recent Progresses on Defect Passivation toward Efficient Perovskite Solar Cells. *Adv. Energy Mater.* **2020**, *10*, 1902650.

(23) Xie, J.; Ping, H.; Tan, T.; Lei, L.; Xie, H.; Yang, X.-Y.; Fu, Z. Bioprocess-Inspired Fabrication of Materials with New Structures and Functions. *Prog. Mater. Sci.* **2019**, *105*, 100571.

(24) Yang, Y.; Kushima, A.; Han, W.; Xin, H.; Li, J. Liquid-Like, Self-Healing Aluminum Oxide during Deformation at Room Temperature. *Nano Lett.* **2018**, *18*, 2492−2497.

(25) Aburto, J.; Moran, M.; Galano, A.; Torres-García, E. Non-Isothermal Pyrolysis of Pectin: A Thermochemical and Kinetic Approach. *J. Anal. Appl. Pyrolysis* **2015**, *112*, 94−104.

(26) Yang, H.; Yan, R.; Chen, H.; Lee, D. H.; Zheng, C. Characteristics of Hemicellulose, Cellulose and Lignin Pyrolysis. *Fuel* **2007**, *86*, 1781−1788.

(27) Li, T.; Chen, Z.; Wang, Y.; Tu, J.; Deng, X.; Li, Q.; Li, Z. Materials for Interfaces in Organic Solar Cells and Photodetectors. *ACS Appl. Mater. Interfaces* **2020**, *12*, 3301−3326.